

Microscopic origin of coercivity enhancement by dysprosium substitution into neodymium permanent magnets


Masamichi Nishino ^{1,2,*}, Hiroshi Hayasaka ², and Seiji Miyashita ^{2,3,4}

¹Research Center for Advanced Measurement and Characterization, National Institute for Materials Science, 1-2-1 Sengen, Tsukuba, Ibaraki 305-0047, Japan

²Elements Strategy Initiative Center for Magnetic Materials, National Institute for Materials Science, 1-2-1 Sengen, Tsukuba, Ibaraki 305-0047, Japan

³Institute for Solid State Physics, The University of Tokyo, 5-1-5 Kashiwanoha, Kashiwa 277-8581, Japan

⁴The Physical Society of Japan, 2-31-22 Yushima, Tokyo 113-0033, Japan

 (Received 9 March 2022; revised 5 August 2022; accepted 5 August 2022; published 17 August 2022)

Neodymium (Nd) magnets ($\text{Nd}_2\text{Fe}_{14}\text{B}$), known as the strongest permanent magnets, are indispensable in realizing high efficiency in energy conversion devices. To enhance their coercivity at high temperatures, the Nd component is substituted with dysprosium (Dy) in the commercial products of the magnet. Surface Dy-rich shells are considered important for enhancing coercivity. However, the underlying microscopic mechanism has not been studied based on atomistic theories. In this study, first, the features and mechanisms of the enhancement were studied using an atomistic model of the Nd magnet. Subsequently, the threshold field (coercive force) for magnetization reversal and the dynamical features at absolute zero and finite temperatures were investigated. The results show that a change from surface to bulk nucleation occurs when the number of substituted layers increases and the anisotropy energy of Dy is resistant to temperature increase, which significantly enhances coercivity, especially at high temperatures.

DOI: [10.1103/PhysRevB.106.054422](https://doi.org/10.1103/PhysRevB.106.054422)

I. INTRODUCTION

High-efficiency energy conversion devices have become central to the efforts to meet increasing energy demands and realize a low-carbon society, for which high-coercivity permanent magnets are key. The strongest permanent magnets, and consequently the most suited for such devices, are neodymium (Nd) magnets, $\text{Nd}_2\text{Fe}_{14}\text{B}$ [1–9], which are widely used in appliances such as electric motors, generators, compressors, and other electronic devices [10]. Although numerous studies on higher coercivity at higher temperatures have been undertaken [11], the origin of coercivity is not well understood.

The Nd magnet comprises grains of hard magnets and grain boundary regions [12–19], and the properties of the surfaces of grains significantly affect coercivity because surface nucleation of the hard magnet triggers magnetization reversal [20]. The coercivity of the Nd magnet is considerably reduced at temperatures above room temperature. However, it is often enhanced by the partial substitution of Nd atoms with dysprosium (Dy) atoms. It was experimentally demonstrated that the anisotropy field of the system, $(\text{Nd}_{1-x}\text{Dy}_x)_2\text{Fe}_{14}\text{B}$, increases with increasing x , leading to an enhancement in the coercive force. Using the method of grain boundary diffusion process, the coercivity is enhanced without losing remanence [21–25]. Consequently, Dy-rich shells are formed between the grain boundary and core Nd magnet in each grain [25]. The formation of Dy-rich shells is considered to play an important role in reinforcing the coercivity.

Micromagnetics coarse-grained model studies suggested that a Dy shell enhances coercivity, and magnetization reversal starts at a grain boundary junction without a Dy shell, while it starts inside a grain with a Dy shell analyzing the saddle point of total energy [26,27]. However, the microscopic origin of the coercivity enhancement, especially at high temperature, is not well understood.

Micromagnetic simulations based on continuum magnetic models with macroscopic magnetic parameters are an effective method used to analyze magnetization reversals and estimate coercive force [28]. This method has an advantage of treating a large system. However, the microscopic details of crystal structures and magnetic parameters are ignored. Furthermore, because of coarse graining, the thermal fluctuation effect is difficult to treat. To understand the microscopic mechanisms of coercivity at finite temperatures, an atomistic model approach is necessary. This approach for the Nd magnet has recently been developed and extensively studied [17,29–43]. In the modeling, the microscopic details of the magnetic parameters and lattice structures are realistically treated, and the temperature effect, including thermal fluctuation, is properly considered [44,45].

Using this approach, not only the qualitative but also quantitative finite-temperature properties were clarified for the magnetization [29–32,39] and domain wall profiles [30,32,33,39,40], spin-reorientation transition [29,30,34], dipolar-interaction effect [31], ferromagnetic resonance [34], inhomogeneity effect [17,33,37,38,40,41], coercive force [35,36], and surface Nd anisotropy effect [43].

In the present study, we show a quantitative estimation of the coercivity and nucleation dynamics of the Nd magnet

*Corresponding author: nishino.masamichi@nims.go.jp

with Dy substitution by the stochastic Landau-Lifshitz-Gilbert (SLLG) method [44,45] using an atomistic model of the Nd magnet, in which the microscopic parameters were primarily taken from first-principles calculations. We examine the microscopic features and origin of the enhancement of the coercivity by Dy substitution.

The rest of the paper is organized as follows. In Sec. II, the model and method are given. In Sec. III A, the threshold field for magnetization reversal is analyzed, and in Sec. III B, the dynamical feature of the nucleation in magnetization reversal is presented, and discussion about the origin of the coercivity enhancement is given. Section IV is devoted to the summary.

II. MODEL AND METHOD

A. Atomistic Hamiltonian for Nd₂Fe₁₄B

The following atomistic Hamiltonian was employed for the Nd magnet with Dy substitution:

$$\mathcal{H} = - \sum_{i<j} 2J_{ij} \mathbf{s}_i \cdot \mathbf{s}_j - \sum_i^{\text{Fe}} D_i (s_i^z)^2 + \sum_i^{\text{R}} \sum_{l,m} \Theta_{l,i} A_{l,i}^m \langle r^l \rangle_i \hat{O}_{l,i}^m - h \sum_i S_i^z. \quad (1)$$

Here, J_{ij} is the exchange interaction between the i th and j th atoms. D_i is the anisotropy constant for the i th Fe atom. The third term is the crystal electric field (CEF) energy of rare earth atoms (Nd and Dy), and $\Theta_{l,i}$, $A_{l,i}^m$, $\langle r^l \rangle_i$, and $\hat{O}_{l,i}^m$ are the Stevens factor, coefficient of the spherical harmonics of the crystalline electric field, average of r^l over the radial wave function, and Stevens operator, respectively. The fourth term is the Zeeman term, and h is the external magnetic field. We consider $l = 2, 4, 6$ and $m = 0$ (diagonal operators), which provide the dominant contribution. For Fe and B atoms, s_i denotes the magnetic moment at the i th site, but for Nd and Dy atoms, s_i is the moment of the valence ($5d$ and $6s$) electrons, which is strongly coupled to the moment of the $4f$ electrons, $\mathcal{J}_i = g_{\text{T}} \mathbf{J}_i / \mu_{\text{B}}$ [Figs. 1(a) and 1(b) for Nd and Dy, respectively], where g_{T} is the Landé g factor and \mathbf{J}_i is the total angular momentum. Thus the total moment for each rare-earth atom is $\mathbf{S}_i = \mathbf{s}_i + \mathcal{J}_i$. For Nd atoms, $J = \mathcal{L} - \mathcal{S} = 9/2$ and $g_{\text{T}} = 8/11$, where \mathcal{L} is the orbital angular momentum, \mathcal{S} is the spin angular momentum and in Dy atoms, $J = \mathcal{L} + \mathcal{S} = 15/2$ and $g_{\text{T}} = 4/3$. For the Fe and B atoms, we define $\mathbf{S}_i = \mathbf{s}_i$. It should be noted that s_i of a Nd (Dy) atom and $\mathbf{S}_i (= s_i)$ of an Fe atom are coupled antiferromagnetically, but \mathbf{S}_i of an Nd atom and that of an Fe atom are coupled ferromagnetically. In contrast \mathbf{S}_i of a Dy atom and that of an Fe atom are coupled antiferromagnetically [Figs. 1(a) and 1(b)].

Magnetic moments and the exchange interactions (the range of $r = 3.52 \text{ \AA}$) were estimated using the Korringa-Kohn-Rostoker (KKR) first-principles method [42,46].

Figure 2 shows the exchange interactions as a function of the distance r between Nd and Fe atoms in Nd₂Fe₁₄B and those between Dy and Fe atoms in Dy₂Fe₁₄B estimated in Ref. [47] by the KKR method. Surprisingly the exchange interactions between Dy and Fe atoms and those between Nd and Fe were found very close. The values of s_i were also very close between the two systems. It is reasonable to consider

that if Nd atoms are substituted by Dy atoms in Nd₂Fe₁₄B, the exchange interactions hardly change. Therefore, the exchange couplings in Nd₂Fe₁₄B were used when an Nd atom is substituted by a Dy atom. D_i for Fe atoms (six types) estimated in a first-principles study [48] were adopted, and for Nd and Dy atoms, $A_{l,i}^m$ given by Yamada *et al.* [49] for R₂Fe₁₄B were applied with $\langle r^l \rangle$ in Ref. [50]. The anisotropy energy of Dy (and Nd) is expected to hardly change in the system with substitution, because it is surrounded by Fe atoms and $4f$ electrons contribute to the anisotropy, while $5d$ and $6s$ electrons to the exchange interaction.

In our previous studies on Nd₂Fe₁₄B [29–31], we obtained the spin-reorientation transition temperature, $T_{\text{R}} = 150 \text{ K}$, which is close to the experimentally estimated temperature [7–9,49] and the critical temperature $T_{\text{C}} \sim 850 \text{ K}$, which is slightly overestimated in comparison to the experimental values $T_{\text{C}} \sim 600 \text{ K}$ [4,7]; thus, we consider the temperature in the scaled form T/T_{C} .

B. Dy substitution

We studied the threshold field for magnetization reversal under an external reversed field as a function of the number of Dy-substituted layers. For this purpose, we focused on the effect of Dy substitution at the (001) surface of the hard magnet on the coercivity in two systems (A and B). In system A, the surface [top ($n = 1$) and bottom ($n = 19$)] layers were in contact with vacuum [Fig. 1(c)], whereas in system B, the surface layers were in contact with a soft magnet (grain boundary) phase [Fig. 1(d)]. We used an open boundary condition along the c axis in system A and periodic boundary condition in system B. The hard (soft) magnet part comprised $12 \times 12 \times 9$ ($12 \times 12 \times 3$) unit cells along the a , b , and c axes, respectively. [The size is $10.56 \text{ nm} \times 10.56 \text{ nm} \times 10.971 \text{ nm}$ ($10.56 \text{ nm} \times 10.56 \text{ nm} \times 3.657 \text{ nm}$).] In both systems, periodic boundary conditions were applied along the a and b axes. The layer of Nd atoms in the hard magnet was numbered as $n = 1, 2, \dots$ in Figs. 1(c) and 1(d). All Nd atoms from the first to the n th layer were substituted with Dy atoms.

The grain boundary phase shows several amorphous-like structures which depend on experimental conditions, and it is difficult to estimate theoretically microscopic parameters of the grain boundary phase. First-principles investigations for the structures have just begun [51,52]. Microscopic magnetic parameters are not available at this moment. Thus we adopted the same crystal structure as in the hard magnet phase, but with smaller magnetic parameters as were used in micromagnetic simulations for Nd magnets: all exchange interactions and anisotropy energies were half and one-fifth, respectively, in the soft magnet phase. The important fact is that it has weak magnetic interactions, and we can capture important features with this modeling.

C. Dynamical method

We investigated magnetization reversal by applying the SLLG equation [44,45],

$$\frac{d}{dt} \mathbf{S}_i = - \frac{\gamma}{1 + \alpha_i^2} \mathbf{S}_i \times \mathbf{h}_i^{\text{eff}} - \frac{\alpha_i \gamma}{(1 + \alpha_i^2) S_i} \mathbf{S}_i \times [\mathbf{S}_i \times \mathbf{h}_i^{\text{eff}}], \quad (2)$$

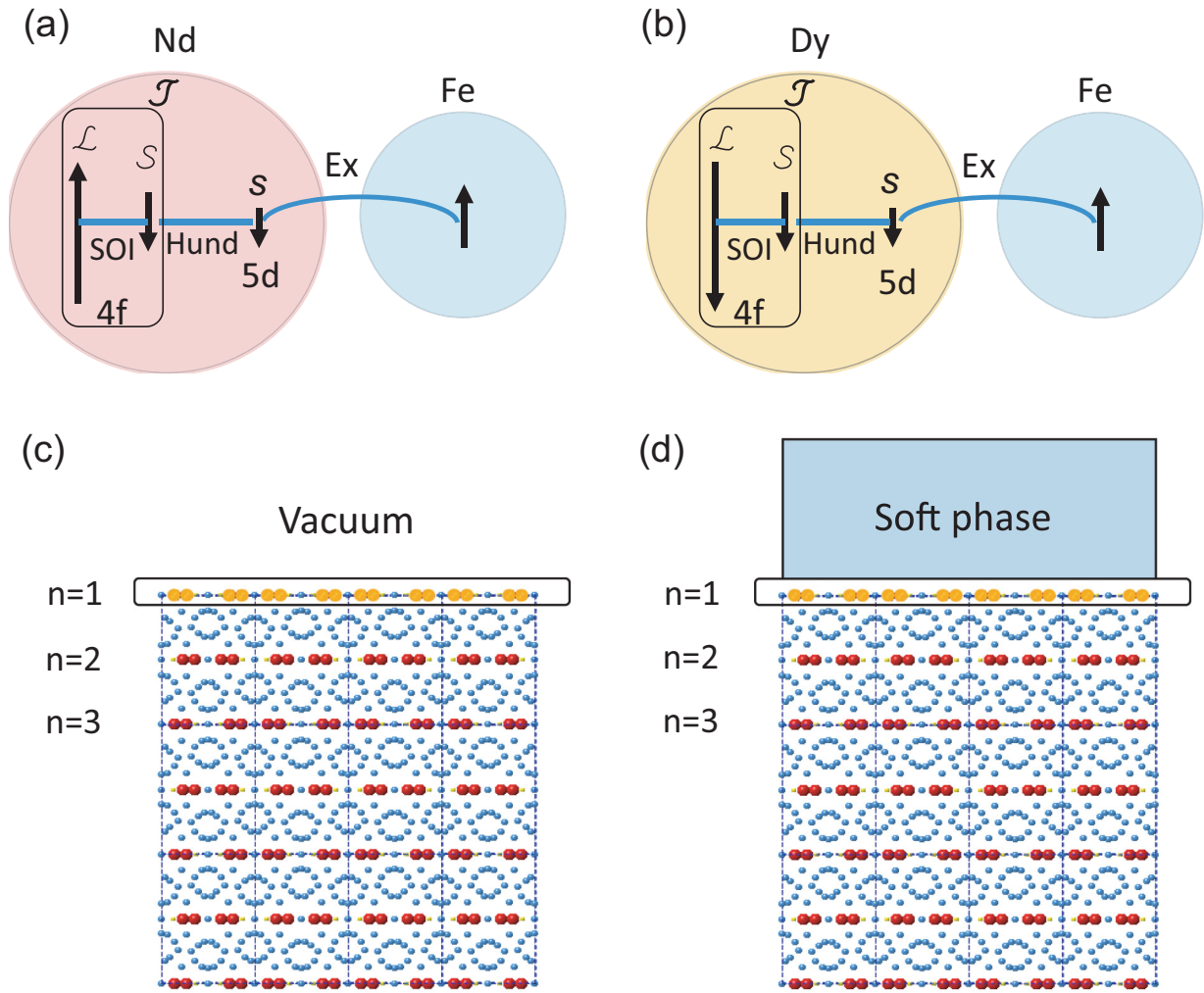


FIG. 1. (a) Magnetic coupling between Nd and Fe atoms. The total moment in an Nd atom and that in an Fe atom are ferromagnetically coupled. Ex and SOI represent the exchange interaction and spin-orbit interaction, respectively. (b) Magnetic coupling between Dy and Fe atoms. The total magnetic moment of a Dy atom and that of an Fe atom are antiferromagnetically coupled. (c) System A. The Nd surface layers were in contact with vacuum. In this example, Nd atoms (red) in the first Nd layer were substituted by Dy atoms (orange). The Nd layers are numbered as $n = 1, 2, \dots$ (d) System B. The Nd surface layers were in contact with a soft magnet phase.

where γ denotes the electron gyromagnetic ratio and α_i is the damping parameter. The effective field $\mathbf{h}_i^{\text{eff}}$ on the i th spin is

$$\mathbf{h}_i^{\text{eff}} = -\frac{\partial \mathcal{H}}{\partial \mathbf{S}_i} + \boldsymbol{\xi}_i(t). \quad (3)$$

Here, the thermal effect is given by the white Gaussian noise field, $\boldsymbol{\xi}_i(t) = (\xi_i^x, \xi_i^y, \xi_i^z)$, which satisfies the following relations:

$$\langle \xi_i^\mu(t) \rangle = 0, \quad \langle \xi_i^\mu(t) \xi_j^\nu(s) \rangle = 2\mathcal{D}_i \delta_{ij} \delta_{\mu\nu} \delta(t-s). \quad (4)$$

The temperature T is controlled employing the fluctuation dissipation relation,

$$\mathcal{D}_i = \frac{\alpha_i k_B T}{\gamma S_i}, \quad (5)$$

where T is proportional to the amplitude of the noise \mathcal{D}_i . With this relation, the system relaxes to a steady state (equilibrium) given by the canonical distribution at temperature T .

To solve Eq. (2) numerically, we applied a middle-point method [45] equivalent to the Heun method for numerical integration with the time step, $\Delta t = 0.1$ fs. α_i is unknown for

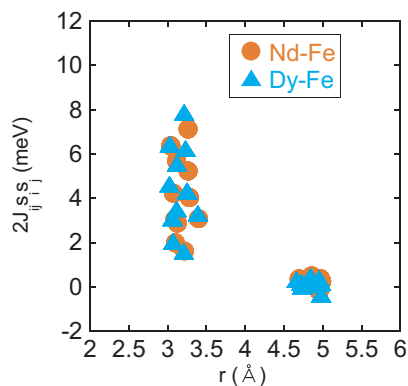


FIG. 2. Exchange interactions between R and Fe atoms in $\text{R}_2\text{Fe}_{14}\text{B}$ as a function of the distance r . R is Nd or Dy.

the Nd magnet, and $\alpha_i = 0.1$ is used [28]. However, this does not affect the results in the present study because the value of α_i has little effect on the threshold field [36].

Subsequently, we simulated the time evolution of magnetization,

$$M_z = \sum_i S_{i,z}, \quad (6)$$

starting from an all-down-spin state under a given value of magnetic field h in the c direction and observe the magnetization reversal. Here, the time of reversal is defined as the point at which the magnetization changes its sign. In the absence of thermal fluctuation at absolute zero, magnetization reversal is a deterministic process. Thus the value of the magnetic field at which the potential barrier vanishes gives the threshold field for magnetization reversal, i.e., the coercive field. At finite temperatures, however, magnetization reversal occurs in a stochastic process and jumps over the energy barrier by virtue of thermal fluctuations. Thus we define the threshold magnetic field at finite temperatures as follows. Twelve simulations were performed with different random number sequences at a given magnetic field value. Then, the number (N) of the case in which magnetization reversal occurred within a simulation time t_{\max} was counted. If $N = 0$, the field is smaller than the threshold field, whereas if $N = 12$, the field is larger than the threshold field. Considering these parameters, we defined the threshold field as the middle point of the interval between the upper limit of the field for $N = 0$ and the lower limit of the field for $N = 12$. The error bar for the threshold field is defined as the interval region of the field. We set $t_{\max} = 0.5$ ns (5×10^6 time steps).

Generally, the threshold field depends on the simulation time. In experiments, the coercivity is a phenomenon of the order of 1 s. However, this is not practical for real-time simulations. Considering that the dependence of the reversal time on the external field around the threshold field is extremely steep, i.e., the reversal time increases exponentially, the estimated threshold fields in this study provide approximate coercive fields. In fact, in our previous paper [36], we estimated that the threshold field for 1 s is approximately 25% less than that of the simulation for 0.5 ns in an Nd magnet system of a similar size.

III. RESULTS

A. Effect of Dy substitution on the threshold field

Figures 3(a)–3(d) show the layer number (n) dependence of the threshold field (orange lines) in system A at $T = 0$, $0.34T_C$, $0.46T_C$, and $0.69T_C$, respectively. Here, $0.46T_C$ is close to room temperature, $0.46T_C \simeq T_{\text{room}}$. $n = 0$ is defined as the case devoid of substitution with Dy atoms, i.e., the original Nd magnet. The value (percentage) for each symbol in the figures denotes the ratio of the threshold field to that for $n = 0$. As reference data, the n dependence of the threshold field (green lines) at each temperature for the system is plotted, in which the anisotropy energy of the surface Nd atoms is doubly reinforced (CEF energy is doubled), as studied in Ref. [43].

We observed that the threshold field increased with n at all temperatures (orange lines), and Dy substitution enhanced

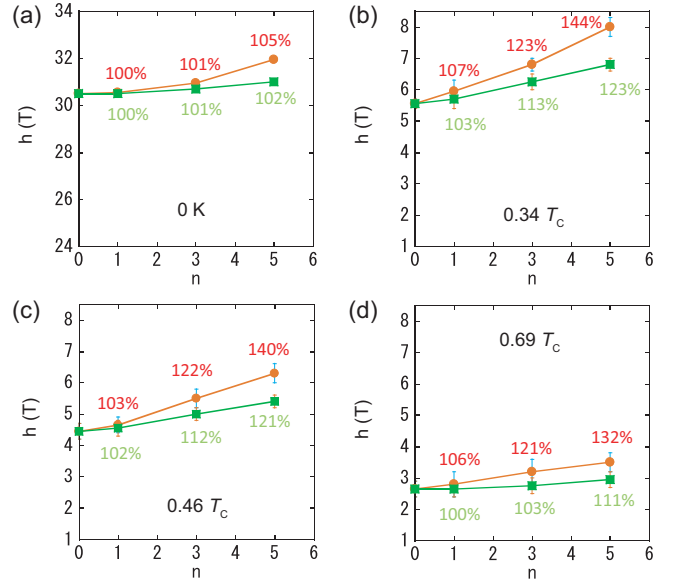


FIG. 3. n dependence of the threshold field (red lines) in system A at (a) 0 K, (b) $0.34T_C$, (c) $0.46T_C$, and (d) $0.69T_C$, compared to the threshold field (green lines) for surface Nd atoms with doubly reinforced anisotropy [43].

the threshold field. Compared to the threshold fields at zero temperature, those at finite temperatures were significantly reduced, and the thermal effect essentially affected the coercivity. The increment ratios of the threshold field as a function of n at finite temperatures were considerably larger than those at zero temperature. Dy substitution had only a marginal effect on the coercivity at zero temperature, whereas it had a relatively large effect at finite temperatures. This tendency is similar to that observed in the system with doubly reinforced anisotropy for surface Nd atoms in a previous study [43]. This indicates that the effect of surface modification with Dy substitution is insignificant at zero temperature because of the Stoner-Wohlfarth mechanism, i.e., simultaneous rotation of all magnetic moments. In contrast this effect is important at finite temperatures because the nucleation mechanism is significant.

We determined that the threshold fields at finite temperatures increased almost linearly with n , and the threshold field at each n was considerably larger than that in the reference system with doubly reinforced anisotropy energy (green lines) in surface Nd atoms. This indicates that Dy substitution strongly enhances the coercivity.

We also discovered that the increment ratio of the threshold field with n was lower at higher temperatures because the thermal fluctuation smears the enhancement effect. However, the enhancement effect of Dy substitution is strong, particularly at high temperatures. This is confirmed by the following observation: in the reference system with surface Nd atoms with doubly reinforced anisotropy, the increment ratios for $n = 5$ were 123%, 121%, and 111% at $0.34T_C$, $0.46T_C$, and $0.69T_C$, respectively. In contrast, in the system with Dy substitution, the ratios were 144%, 140%, and 132%, respectively, which exhibited lower reductions in the ratio at high temperatures. This distinctly indicates that Dy substitution suppresses the decrease in coercivity due to thermal fluctuation.

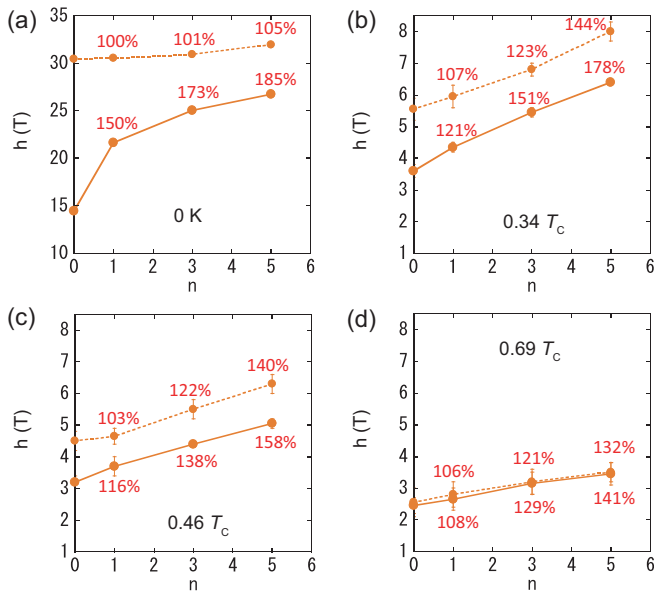


FIG. 4. n dependence of the threshold field (solid lines) in system B at (a) 0 K, (b) $0.34T_C$, (c) $0.46T_C$, and (d) $0.69T_C$. Those in system A (dotted lines) are also plotted for comparison.

Figures 4(a)–4(d) depict n dependence of the threshold field (solid lines) in system B at $T = 0, 0.34T_C, 0.46T_C$, and $0.69T_C$, respectively, in comparison to the corresponding threshold field in system A (dotted lines). The value (percentage) for each symbol in the Figs. denotes the ratio of the threshold field to that for $n = 0$. Here, we observed that the grain boundary phase (soft magnet) significantly affected the coercivity and reduced it, except in case (d) at $T = 0.69T_C$. Owing to the small anisotropy energies and exchange interactions in the grain boundary phase, prior to the magnetization reversal of the hard magnet phase, the moments in the grain boundary phase are reversed, and a domain wall is generated around the interface between the soft and hard magnets. When this domain wall propagates to the hard magnet phase, surface nucleation occurs in the grain, thereby leading to magneti-

zation reversal. This process occurs more easily than surface nucleation in system A.

However, we found that Dy substitution enhanced the coercivity more intensely in system B than in system A. For example, at $0.46T_C \simeq T_{\text{room}}$, one-layer Dy substitution ($n = 1$) had almost no effect (103%) on the threshold field in system A, while it had an effect (116%) in system B. Moreover, the increment ratios for all n in system B were larger than those in system A. This tendency was observed at all temperatures. This indicates that Dy substitution is effective for the suppression of domain wall propagation to the grain phase, and it has a strong effect of the domain wall pinning.

At $0.69T_C$, the soft magnet phase is paramagnetic owing to the half strength of the exchange interaction, and the moments in the hard magnet phase fluctuate owing to the high temperature. Thus the effect of the soft magnet phase is insignificant for the surface nucleation in the hard magnet, i.e., magnetization reversal, leading to similar dependence between systems A and B. At zero temperature, Dy substitution had only a marginal effect on the coercivity in system A. In contrast, in system B, the increase of the coercivity with n is significant, and the Dy layers resist the domain wall propagation efficiently.

Finally, we determined that the threshold fields at finite temperatures increased almost linearly with n , and the slope of the increment of the threshold field for all temperatures in system B was nearly identical to that in system A. Furthermore, it can be concluded that Dy substitution enhances the coercive force by a ratio proportional to the number of substituted layers.

B. Nucleation feature

To investigate the microscopic mechanism of coercivity enhancement by Dy substitution, we analyzed the dynamical features of the nucleation in the magnetization reversal at $0.46T_C \simeq T_{\text{room}}$. Figures 5(a) and 5(b) exhibit snapshots of the spin configuration in nucleation for $n = 1$ and 5 at threshold fields $h = 4.65$ and 6.30 T, respectively, in system A (see also animation_An1 and animation_An5 for detailed features in Ref. [53]). Here, the red and blue parts indicate the up-spin

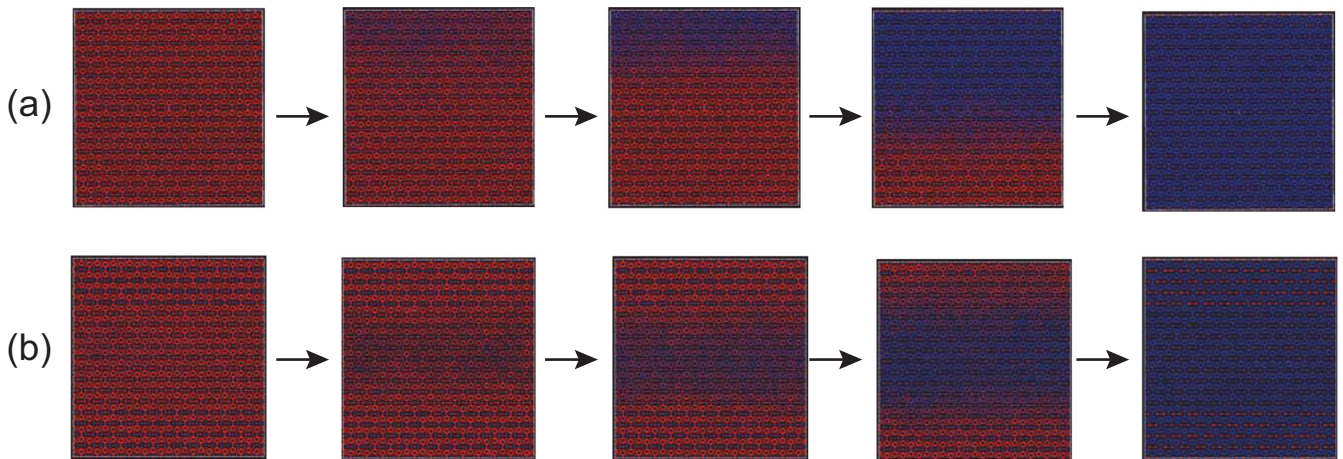


FIG. 5. Snapshots of the spin configuration in nucleation for (a) $n = 1$ and (b) 5 at the threshold fields $h = 4.65$ and 6.30 T, respectively, at $0.46T_C \simeq T_{\text{room}}$ in system A. Red and blue parts denote up-spin and down-spin ones.

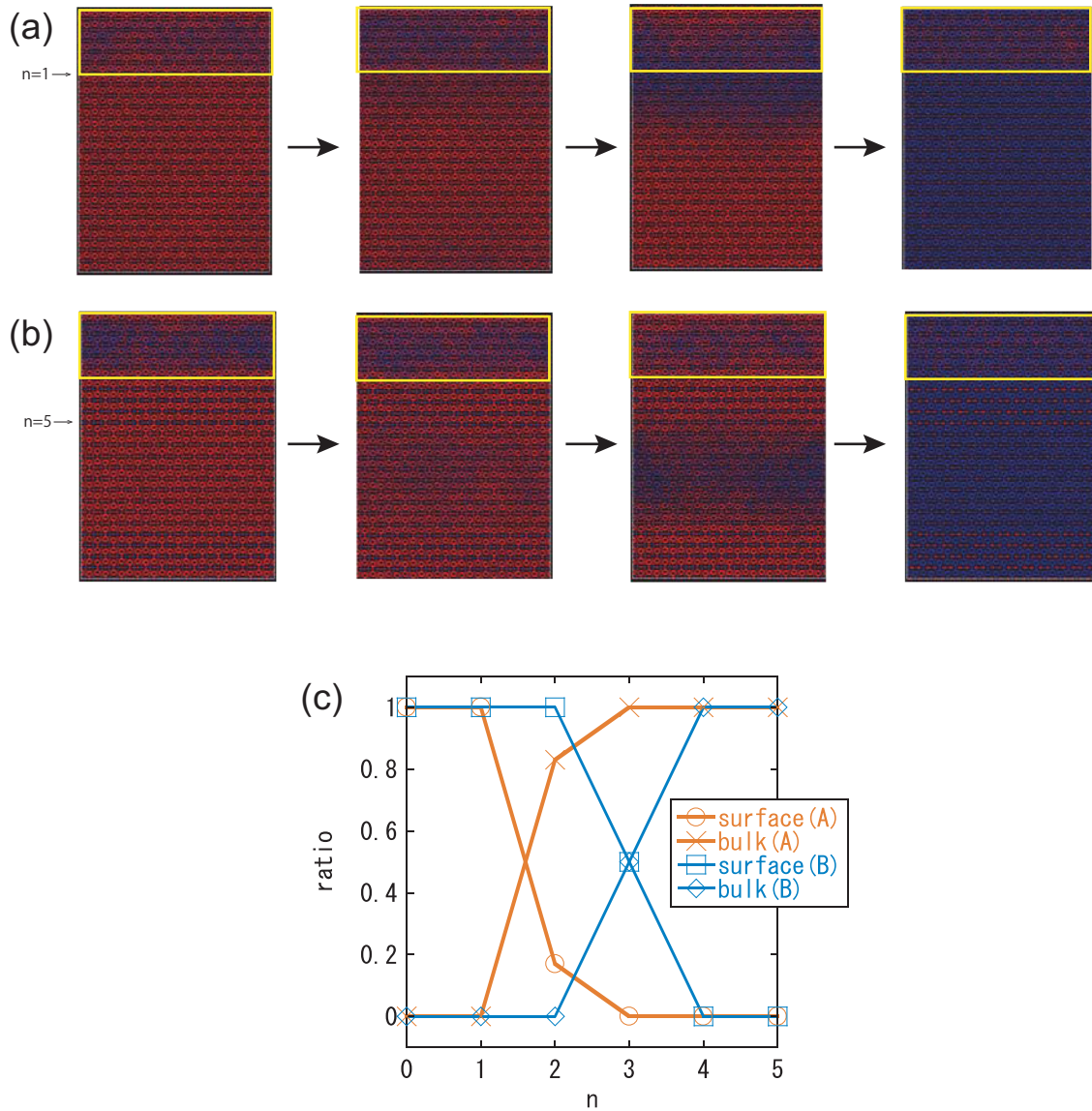


FIG. 6. Snapshots of the spin configuration in nucleation for (a) $n = 1$ and (b) 5 at the threshold fields $h = 3.70$ and 5.05 T, respectively, at $0.46T_C \simeq T_{\text{room}}$ in system B. The yellow-boxed regions correspond to the soft magnet phase. (c) Ratios of surface and bulk nucleation as functions of n in systems A and B at $0.46T_C \simeq T_{\text{room}}$.

state and down-spin state, respectively. In the case of $n = 1$, nucleation occurs from the surface and the domain rapidly grows in the direction of the a or b axis, and then proceeds in the direction of the c axis. In contrast to this feature, we found that in Fig. 5(b), the nucleation pattern radiates outwards from inside the system for $n = 5$.

Figures 6(a) and 6(b) depict snapshots of the spin configuration in nucleation for $n = 1$ and $n = 5$ at the threshold fields $h = 3.70$ and 5.05 T, respectively, in system B (see also animation_Bn1 and animation_Bn5 for detailed features in Ref. [53]). Prior to nucleation in the hard magnet phase, a large part of the magnetic moments in the soft magnet phase was reversed, and a domain wall was generated around the interface. We discovered that for $n = 1$, nucleation occurs at the interface, and surface nucleation occurs in the hard magnet phase. However, as shown in Fig. 6(b), for $n = 5$, nucleation is initiated on the inside of the hard magnet. Thus

it can be concluded that if n is sufficiently large, the nucleation mechanism changes from surface nucleation to bulk nucleation.

In addition, we investigated the critical value of n to distinguish between surface and bulk nucleation. Figure 6(c) presents the ratios between the surface and bulk nucleation at the threshold fields as functions of n in systems A and B at $0.46T_C \simeq T_{\text{room}}$. We observed the numbers of surface and bulk nucleation in six samples of reversal for each system and estimated the ratios.

We also established that in case A, for $n \leq 1$, surface nucleation occurs, $n = 2$ is critical, and for $n \geq 3$, bulk nucleation occurs. In contrast, in case B, for $n \leq 2$, surface nucleation occurs, $n = 3$ is critical, and for $n \geq 4$, bulk nucleation occurs. This indicates that the domain wall helps surface nucleation in the grain, and a larger n is needed for bulk nucleation in case B.

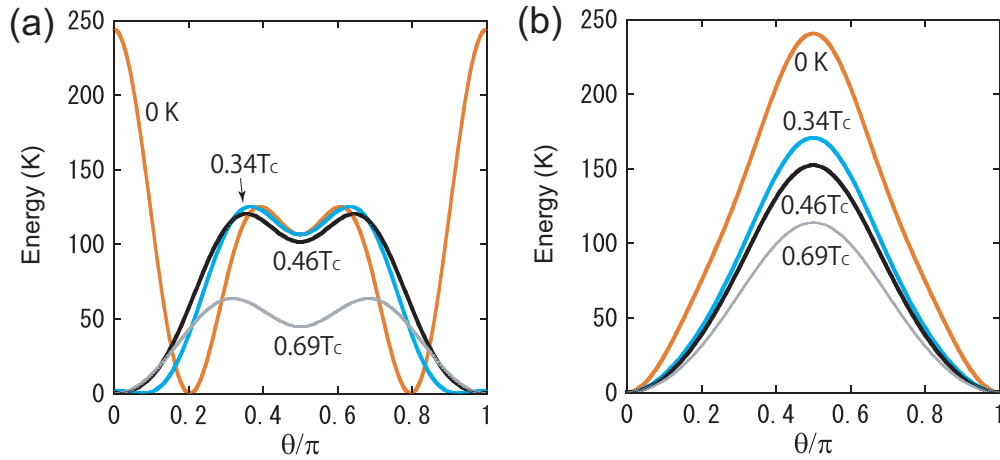


FIG. 7. (a) Crystal electric field energy for a Nd atom as a function of θ at zero and finite temperatures. (b) Crystal electric field energy for a Dy atom as a function of θ at zero and finite temperatures.

Subsequently, we considered the origin of the strong enhancement effect of Dy substitution. The magnetic coupling between the moments of Nd and Fe atoms is ferromagnetic, whereas that between Dy and Fe is antiferromagnetic [Figs. 1(a) and 1(b)]. This antiferromagnetic coupling stabilizes the moments of Dy atoms and the nucleation in this region is suppressed.

Another important component is the property of magnetic anisotropy, i.e., the CEF energy,

$$\mathcal{H}_{\text{CEF}} = \sum_{l,m} B_l^m \hat{O}_l^m, \quad (7)$$

where $B_l^m = \Theta_l A_l^m(r^l)$. The Stevens operator, \hat{O}_l^m , is a function of the z component of \mathbf{J} , that is, J_z . At finite temperatures, the moment J_z shrinks due to the thermal fluctuation as $J_z = CJ \cos \theta$ with $0 < C < 1$. The coefficient C is estimated to be $C \simeq 0.83, 0.76$, and 0.62 at $T = 0.34T_c, 0.46T_c$, and $0.69T_c$, respectively, in the bulk of $\text{Nd}_2\text{Fe}_{14}\text{B}$ from the temperature dependence of the magnetization in our previous study [30]. Substituting $J_z = CJ \cos \theta$ into Eq. (7) for an Nd atom, we obtain the temperature dependence of the effective CEF energy for an Nd atom, as shown in Fig. 7(a). The CEF energy has a minimum at $\theta \simeq 0.2\pi$ at 0 K but $\theta = 0$ at finite temperatures, which is the origin of the spin-reorientation (SR) transition. Because it is difficult to estimate how much J_z is reduced in a Dy atom in systems with Dy substitution, we assume that the same ratio is reduced in Dy atoms in the systems. Substituting $J_z = CJ \cos \theta$ into Eq. (7) for a Dy atom with the same ratios as the Nd atom, we illustrate the temperature dependence of the CEF energy in Fig. 7(b).

Furthermore, we determined that the CEF energy has a minimum at $\theta = 0$ regardless of temperature, and a considerably higher potential barrier than that of the Nd atom for all temperatures. Thus we conclude that this difference causes an enhancement of the coercivity with Dy substitution. In addition, we noticed that the difference in the potential barrier between Nd and Dy atoms is relatively larger at $0.69T_c$ than at $0.46T_c$. This can be inferred from the observation that the energy barrier of a Dy atom is 27% higher than that of a Nd atom at $0.46T_c$, whereas it is 79% higher at $0.69T_c$. This

indicates that Dy substitution is more effective at temperatures higher than room temperature.

IV. SUMMARY

We studied the microscopic origin of the coercivity enhancement by Dy substitution. We examined quantitative dependence of the coercivity enhancement on Dy substitution applying the atomistic model to two systems: system A, which was in contact with vacuum and system B, which was in contact with the soft magnet phase.

We discovered that the effect of Dy substitution at finite temperatures is considerably stronger than that at absolute zero, where the underlying mechanism of magnetization reversal is the Stoner-Wohlfarth mechanism, whereas at finite temperatures it is the nucleation mechanism. We demonstrated that Dy substitution significantly enhances coercivity, and this effect is considerably larger than that of doubly reinforced anisotropy energy for surface Nd atoms, especially at temperatures higher than room temperature.

Furthermore, we established that the enhancement ratio of the threshold field by Dy substitution is nearly proportional to the number of substituted layers in both systems A and B at finite temperatures, and that the grain boundary phase (soft magnet) significantly reduces the coercivity. However, Dy substitution is found to be more effective in system B, which indicates that Dy substitution effectively suppresses the propagation of a domain wall into the grain phase.

In addition, we clarified that when the number of substituted layers increases, the nucleation mechanism changes, thereby causing coercivity enhancement. We first demonstrated it explicitly showing nucleation dynamics (time-dependent dynamics). The surface nucleation is suppressed by increasing the number (n) of the substituted layers, and at a critical n , the crossover between surface and bulk nucleation occurs. To be precise, for $n > n_c$, bulk nucleation occurs. It is noteworthy, however, that the critical value of n_c in system B was larger than that in system A.

The coercivity enhancement by Dy substitution is considered to originate primarily from two sources. One is the

antiferromagnetic coupling between the moments of Dy and Fe atoms, which increases the stability of the surface state against the external reversed field. The other is the feature of the CEF energy of a Dy atom. The minimum CEF energy of a Dy atom is located at $\theta = 0$ at all temperatures, whereas that of an Nd atom is located at $\theta \simeq 0.2\pi$ at 0 K and at $\theta = 0$ at finite temperatures above the SR transition temperature. Furthermore, the potential barrier for a Dy atom is higher than that for an Nd atom, especially at high temperatures. This explains the effectiveness of Dy substitution for high-temperature usage of Nd magnets in commercial products.

We performed Dy substitution for all Nd atoms up to the n th Nd layers. In experimental situations, some spatial distributions of substituted Dy atoms may exist and the percentage of Dy substitution may depend on the depth of the Nd layer, which remain unclarified. However, if the spatial distribution information is experimentally clarified in the future, it can be introduced into our model. This would enable an analysis of the relationship between the Dy distribution and coercivity enhancement that is more quantitative.

The present study is the first to show the features and mechanisms of the coercivity enhancement in the Nd magnet by Dy substitution based on the atomistic viewpoint, which may provide useful information for trials toward enhancement of the coercivity of permanent magnets.

ACKNOWLEDGMENTS

The authors would like to thank Dr. Hirosawa for the instructive discussions concerning the effect of Dy substitution from experimental viewpoints, and Prof. Akai and Dr. Toga for useful discussions on the magnetic parameters for $\text{Dy}_2\text{Fe}_{14}\text{B}$ by the KKR method. This work was supported by the Elements Strategy Initiative Center for Magnetic Materials (ESICMM) (Grant No. 12016013) funded by the Ministry of Education, Culture, Sports, Science and Technology (MEXT) of Japan, and was partially supported by Grants-in-Aid for Scientific Research C (No. 18K03444 and No. 20K03809) from MEXT. Numerical calculations were performed using the Numerical Materials Simulator at the National Institute for Materials Science.

-
- [1] M. Sagawa and S. Hirosawa, Magnetic hardening mechanism in sintered R-Fe-B permanent magnets, *J. Mater. Res.* **3**, 45 (1988).
- [2] J. F. Herbst, J. J. Croat, F. E. Pinkerton, and W. B. Yelon, Relationships between crystal structure and magnetic properties in $\text{Nd}_2\text{Fe}_{14}\text{B}$, *Phys. Rev. B* **29**, 4176 (1984).
- [3] S. Hirosawa, Y. Matsuura, H. Yamamoto, S. Fujimura, M. Sagawa, and H. Yamauchi, Single crystal measurements of anisotropy constants of $\text{R}_2\text{Fe}_{14}\text{B}$ (R = Y, Ce, Pr, Nd, Gd, Tb, Dy and Ho), *Jpn. J. Appl. Phys.* **24**, L803 (1985).
- [4] A. V. Andreev, A. V. Deriagin, N. V. Kudrevatykh, N. V. Mushnikov, and V. A. Reimer, The magnetism of $\text{Y}_2\text{Fe}_{14}\text{B}$ and $\text{Nd}_2\text{Fe}_{14}\text{B}$ and their hydrides, *Zh. Eksp. Teor. Fiz.* **90**, 1042 (1986) [*Sov. Phys. JETP* **63**, 608 (1986)].
- [5] H. Kronmüller, K.-D. Durst, and M. Sagawa, Analysis of the magnetic hardening mechanism in RE-FeB permanent magnets, *J. Magn. Magn. Mater.* **74**, 291 (1988).
- [6] J. F. Herbst, $\text{R}_2\text{Fe}_{14}\text{B}$ materials: Intrinsic properties and technological aspects, *Rev. Mod. Phys.* **63**, 819 (1991).
- [7] S. Hirosawa, Y. Matsuura, H. Yamamoto, S. Fujimura, M. Sagawa, and H. Yamauchi, Magnetization and magnetic anisotropy of $\text{R}_2\text{Fe}_{14}\text{B}$ measured on single crystals, *J. Appl. Phys.* **59**, 873 (1986).
- [8] O. Yamada, Y. Ohtsu, F. Ono, M. Sagawa, and S. Hirosawa, Magnetocrystalline anisotropy in $\text{Nd}_2\text{Fe}_{14}\text{B}$ intermetallic compound, *J. Magn. Magn. Mater.* **70**, 322 (1987).
- [9] N. V. Mushnikov, P. B. Terent'ev, and E. V. Rosenfel'd, Magnetic anisotropy of the $\text{Nd}_2\text{Fe}_{14}\text{B}$ compound and its hydride $\text{Nd}_2\text{Fe}_{14}\text{BH}_4$, *Phys. Metals Metallogr.* **103**, 39 (2007).
- [10] S. Sugimoto, Current status and recent topics of rare-earth permanent magnets, *J. Phys. D* **44**, 064001 (2011).
- [11] T. Akiya, J. Liu, H. Sepehri-Amin, T. Ohkubo, K. Hioki, A. Hattori, and K. Hono, High-coercivity hot-deformed Nd-Fe-B permanent magnets processed by Nd-Cu eutectic diffusion under expansion constraint, *Scr. Mater.* **81**, 48 (2014).
- [12] R. Friedberg and D. I. Paul, New Theory of Coercive Force of Ferromagnetic Materials, *Phys. Rev. Lett.* **34**, 1234 (1975).
- [13] A. Sakuma, S. Tanigawa, and M. Tokunaga, Micromagnetic studies of inhomogeneous nucleation in hard magnets, *J. Magn. Magn. Mater.* **84**, 52 (1990).
- [14] A. Sakuma, The theory of inhomogeneous nucleation in uniaxial ferromagnets, *J. Magn. Magn. Mater.* **88**, 369 (1990).
- [15] S. Mohakud, S. Andraus, M. Nishino, A. Sakuma, and S. Miyashita, Temperature dependence of the threshold magnetic field for nucleation and domain wall propagation in an inhomogeneous structure with grain boundary, *Phys. Rev. B* **94**, 054430 (2016).
- [16] A. L. Wysocki and V. P. Antropov, Micromagnetic simulations with periodic boundary conditions: Hard-soft nanocomposites, *J. Magn. Magn. Mater.* **428**, 274 (2017).
- [17] I. E. Uysal, M. Nishino, and S. Miyashita, Magnetic field threshold for nucleation and depinning of domain walls in the neodymium permanent magnet $\text{Nd}_2\text{Fe}_{14}\text{B}$, *Phys. Rev. B* **101**, 094421 (2020).
- [18] S. Okamoto, R. Goto, N. Kikuchi, O. Kitakami, T. Akiya, H. Sepehri-Amin, T. Ohkubo, K. Hono, K. Hioki, and A. Hattori, Temperature-dependent magnetization reversal process and coercivity mechanism in Nd-Fe-B hot-deformed magnets, *J. Appl. Phys.* **118**, 223903 (2015).
- [19] T. Pramanik, A. Roy, R. Dey, A. Rai, S. Guchhait, H. C. Movva, C.-C. Hsieh, and S. K. Banerjee, Angular dependence of magnetization reversal in epitaxial chromium telluride thin films with perpendicular magnetic anisotropy, *J. Magn. Magn. Mater.* **437**, 72 (2017).
- [20] S. Hirosawa, M. Nishino, and S. Miyashita, Perspectives for high-performance permanent magnets: Applications, coercivity, and new materials, *Adv. Nat. Sci: Nanosci. Nanotechnol.* **8**, 013002 (2017).

- [21] K. Hirota, H. Nakamura, T. Minowa, and M. Honshima, Coercivity enhancement by the grain boundary diffusion process to Nd-Fe-B sintered magnets, *IEEE Trans. Magn.* **42**, 2909 (2006).
- [22] F. Xu, J. Wang, X. Dong, L. Zhang, and J. Wu, Grain boundary microstructure in DyF₃-diffusion processed Nd-Fe-B sintered magnets, *J. Alloys Compd.* **509**, 7909 (2011).
- [23] K. Löwe, C. Brombacher, M. Katter, and O. Gutfleisch, Temperature-dependent Dy diffusion processes in Nd-Fe-B permanent magnets, *Acta Mater.* **83**, 248 (2015).
- [24] W. Chen, J. M. Luo, Y. W. Guan, Y. L. Huang, M. Chen, and Y. H. Hou, Grain boundary diffusion of Dy films prepared by magnetron sputtering for sintered Nd-Fe-B magnets, *J. Phys. D Appl. Phys.* **51**, 185001 (2018).
- [25] T.-H. Kim, T. Sasaki, T. Ohkubo, Y. Takada, A. Kato, Y. Kaneko, and K. Hono, Microstructure and coercivity of grain boundary diffusion processed Dy-free and Dy-containing Nd-Fe-B sintered magnets, *Acta Mater.* **172**, 139 (2019).
- [26] S. Bance, J. Fischbacher, A. Kovacs, H. Oezelt, F. Reichel, and T. Schrefl, Thermal activation in permanent magnets, *JOM* **67**, 1350 (2015).
- [27] J. Fischbacher, A. Kovacs, L. Exl, J. Kühnel, E. Mehofer, H. Sepehri-Amin, T. Ohkubo, K. Hono, and T. Schrefl, Searching the weakest link: Demagnetizing fields and magnetization reversal in permanent magnets, *Scr. Mater.* **154**, 253 (2018).
- [28] H. Kronmüller, M. Fähnle, and C. U. Press, *Micromagnetism and the Microstructure of Ferromagnetic Solids*, Cambridge Studies in Magnetism (Cambridge University Press, Cambridge, UK, 2003).
- [29] Y. Toga, M. Matsumoto, S. Miyashita, H. Akai, S. Doi, T. Miyake, and A. Sakuma, Monte carlo analysis for finite-temperature magnetism of Nd₂Fe₁₄B permanent magnet, *Phys. Rev. B* **94**, 174433 (2016).
- [30] M. Nishino, Y. Toga, S. Miyashita, H. Akai, A. Sakuma, and S. Hirosawa, Atomistic-model study of temperature-dependent domain walls in the neodymium permanent magnet Nd₂Fe₁₄B, *Phys. Rev. B* **95**, 094429 (2017).
- [31] T. Hinokihara, M. Nishino, Y. Toga, and S. Miyashita, Exploration of the effects of dipole-dipole interactions in Nd₂Fe₁₄B thin films based on a stochastic cutoff method with a novel efficient algorithm, *Phys. Rev. B* **97**, 104427 (2018).
- [32] S. Miyashita, M. Nishino, Y. Toga, T. Hinokihara, T. Miyake, S. Hirosawa, and A. Sakuma, Perspectives of stochastic micromagnetism of Nd₂Fe₁₄B and computation of thermally activated reversal process, *Scr. Mater.* **154**, 259 (2018).
- [33] Y. Toga, M. Nishino, S. Miyashita, T. Miyake, and A. Sakuma, Anisotropy of exchange stiffness based on atomic-scale magnetic properties in the rare-earth permanent magnet Nd₂Fe₁₄B, *Phys. Rev. B* **98**, 054418 (2018).
- [34] M. Nishino and S. Miyashita, Nontrivial temperature dependence of ferromagnetic resonance frequency for spin reorientation transitions, *Phys. Rev. B* **100**, 020403(R) (2019).
- [35] Y. Toga, S. Miyashita, A. Sakuma, and T. Miyake, Role of atomic-scale thermal fluctuations in the coercivity, *npj Comput. Mater.* **6**, 67 (2020).
- [36] M. Nishino, I. E. Uysal, T. Hinokihara, and S. Miyashita, Dynamical aspects of magnetization reversal in the neodymium permanent magnet by a stochastic Landau-Lifshitz-Gilbert simulation at finite temperature: Real-time dynamics and quantitative estimation of coercive force, *Phys. Rev. B* **102**, 020413(R) (2020).
- [37] S. Westmoreland, R. Evans, G. Hrkac, T. Schrefl, G. Zimanyi, M. Winklhofer, N. Sakuma, M. Yano, A. Kato, T. Shoji, A. Manabe, M. Ito, and R. Chantrell, Multiscale model approaches to the design of advanced permanent magnets, *Scr. Mater.* **148**, 56 (2018).
- [38] S. C. Westmoreland, C. Skelland, T. Shoji, M. Yano, A. Kato, M. Ito, G. Hrkac, T. Schrefl, R. F. L. Evans, and R. W. Chantrell, Atomistic simulations of α -Fe/Nd₂Fe₁₄B magnetic core/shell nanocomposites with enhanced energy product for high temperature permanent magnet applications, *J. Appl. Phys.* **127**, 133901 (2020).
- [39] Q. Gong, M. Yi, R. F. L. Evans, B.-X. Xu, and O. Gutfleisch, Calculating temperature-dependent properties of Nd₂Fe₁₄B permanent magnets by atomistic spin model simulations, *Phys. Rev. B* **99**, 214409 (2019).
- [40] Q. Gong, M. Yi, and B.-X. Xu, Multiscale simulations toward calculating coercivity of Nd-Fe-B permanent magnets at high temperatures, *Phys. Rev. Materials* **3**, 084406 (2019).
- [41] Q. Gong, M. Yi, R. F. L. Evans, O. Gutfleisch, and B.-X. Xu, Anisotropic exchange in Nd-Fe-B permanent magnets, *Mater. Res. Lett.* **8**, 89 (2020).
- [42] S. Miyashita, M. Nishino, Y. Toga, T. Hinokihara, I. E. Uysal, T. Miyake, H. Akai, S. Hirosawa, and A. Sakuma, Atomistic theory of thermally activated magnetization processes in Nd₂Fe₁₄B permanent magnet, *Sci. Tech. Adv. Mater.* **22**, 658 (2021).
- [43] M. Nishino, I. E. Uysal, and S. Miyashita, Effect of the surface magnetic anisotropy of neodymium atoms on the coercivity in neodymium permanent magnets, *Phys. Rev. B* **103**, 014418 (2021).
- [44] J. L. García-Palacios and F. J. Lázaro, Langevin-dynamics study of the dynamical properties of small magnetic particles, *Phys. Rev. B* **58**, 14937 (1998).
- [45] M. Nishino and S. Miyashita, Realization of the thermal equilibrium in inhomogeneous magnetic systems by the Landau-Lifshitz-Gilbert equation with stochastic noise, and its dynamical aspects, *Phys. Rev. B* **91**, 134411 (2015).
- [46] A. Liechtenstein, M. Katsnelson, V. Antropov, and V. Gubanov, Local spin density functional approach to the theory of exchange interactions in ferromagnetic metals and alloys, *J. Magn. Magn. Mater.* **67**, 65 (1987).
- [47] T. Miyake, Y. Harashima, T. Fukazawa, and H. Akai, Understanding and optimization of hard magnetic compounds from first principles, *Sci. Tech. Adv. Mater.* **22**, 543 (2021), pMID: 34552388.
- [48] Y. Miura, H. Tsuchiura, and T. Yoshioka, Magnetocrystalline anisotropy of the Fe-sublattice in Y₂Fe₁₄B systems, *J. Appl. Phys.* **115**, 17A765 (2014).
- [49] M. Yamada, H. Kato, H. Yamamoto, and Y. Nakagawa, Crystal-field analysis of the magnetization process in a series of Nd₂Fe₁₄B-type compounds, *Phys. Rev. B* **38**, 620 (1988).
- [50] A. J. Freeman and R. E. Watson, Theoretical investigation of some magnetic and spectroscopic properties of rare-earth ions, *Phys. Rev.* **127**, 2058 (1962).
- [51] Y. Tatetsu, S. Tsuneyuki, and Y. Gohda, First-Principles Study of the Role of Cu in Improving the Coercivity of Nd-Fe-B Permanent Magnets, *Phys. Rev. Applied* **6**, 064029 (2016).

- [52] Y. Gohda, Y. Tatetsu, and S. Tsuneyuki, Electron theory on grain-boundary structures and local magnetic properties of neodymium magnets, *Materials Transactions* **59**, 332 (2018).
- [53] See Supplemental Material at <http://link.aps.org/supplemental/10.1103/PhysRevB.106.054422> for a more detailed description of the dynamical method, effect of Dy substitution, nucleation feature, ratio of surface, and bulk nucleation.